Chapter 4

Atg4 proteolytic activity can be inhibited by Atg1 phosphorylation

Jana Sánchez-Wandelmer, Franziska Kriegenburg, Sabrina Rohringer, Martina Schuschnig, Rubén Gómez-Sánchez, Bettina Zens, Susana Abreu, Ralph Hardenberg, David Hollenstein, Jieqiong Gao, Christian Ungermann, Sascha Martens, Claudine Kraft and Fulvio Reggiori

Nature Communications. 18;8(1):295 (2017).

Abstract

The biogenesis of autophagosomes depends on the conjugation of Atg8-like proteins with phosphatidylethanolamine. Atg8 processing by the cysteine protease Atg4 is required for its covalent linkage to phosphatidylethanolamine, but it is also necessary for Atg8 deconjugation from this lipid to release it from membranes. How these two cleavage steps are coordinated is unknown. Here we show that phosphorylation by Atg1 inhibits Atg4 function, an event that appears to exclusively occur at the site of autophagosome biogenesis. These results are consistent with a model where the Atg8-phosphatidylethanolamine pool essential for autophagosome formation is protected at least in part by Atg4 phosphorylation by Atg1 while newly synthesized cytoplasmic Atg8 remains susceptible to constitutive Atg4 processing.

Introduction

Macroautophagy (hereafter autophagy) is highly conserved among eukaryotes, and it is crucial for the maintenance of cellular homeostasis in response to cellular and environmental stresses. This pathway is also essential for a multitude of physiological processes, such as cell differentiation and defense against pathogens, and it is associated with the pathophysiology of several diseases, including cancer and neurodegeneration[1]. During autophagy, double-membrane vesicles called autophagosomes sequester cytoplasmic components and target them to lysosomes/vacuoles for degradation. The resulting metabolites are subsequently recycled back to the cytoplasm and reused for the synthesis of new macromolecules or as a source of energy[2]. In yeast, the orchestrated action of the autophagy-related (Atg) proteins at the phagophore assembly site or pre-autophagosomal structure (PAS) mediates the formation, expansion and sealing of a cistern, known as the phagophore or isolation membrane, to create an autophagosome[2]. The kinase activity of the Atg1 complex, composed by the Atg1 kinase, Atg13, Atg17, Atg29, and Atg31, is a key regulator of this process[3]. Previous studies suggest that sealed autophagosomes cannot fuse with lysosomes/vacuoles until the Atg proteins get dissociated from

autophagosomal membranes[4], which partially depends on phosphatidylinositol-3-phosphate (PI3P) turnover[5,6]. The Ymr1 phosphatase is pivotal in PI3P clearance on autophagosomes, which otherwise accumulate in the cytoplasm in its absence[5]. Although PI3P turnover could be sufficient to release PI3P-binding proteins, such as Atg18 and Atg21[7], an additional mechanism is required for the dissociation of proteins such as Atg8 that are covalently conjugated to membranes. In yeast, Atg4 constitutively cleaves the C-terminal arginine of Atg8[8–10], allowing Atg8 conjugation to the phosphatidylethanolamine (PE) in autophagosomal membranes[2]. Once conjugated to PE, Atg8 is involved in cargo selection and thought to contribute to the expansion and closure of phagophores, possibly by forming a vesicle coat[11–13]. Atg4 also deconjugates Atg8 from PE upon autophagosome completion[9,14]. The release from its PE anchor is essential not only for Atg8 recycling but also, analogously to PI3P turnover, to allow the fusion of autophagosomes with vacuoles[9,15,16]. How Atg8–PE cleavage by Atg4 is timely and spatially regulated, however, is still mysterious. In this study, we describe a novel regulatory mechanism, in which the Atg1 kinase specifically inhibits the deconjugating activity of Atg4 at the PAS, possibly contributing to the protection of the Atg8–PE pool necessary for autophagosome biogenesis.

Results

Atg1 phosphorylates Atg4 and inhibits autophagy. In our search for regulators of Atg4 activity, we made the assumption that this factor should possess two main characteristics, i.e., to be a protein present on autophagosomal membranes and be able to reversibly modify its substrates. The Atg1 kinase fits with this profile, because it dynamically localizes to the PAS[17], and it has been shown that its phosphorylations can be antagonized by phosphatases[18]. Interestingly, the sequence analysis of Atg4 revealed that it contains at least seven putative Atg1 phosphorylation consensus sites (**Supplementary Figure 1a**)[19]. We therefore decided to explore whether Atg4 is a substrate of Atg1. Purified Atg1 complexes containing either Atg1 or kinase-dead

Atg1(Atg1^{D211A}) were incubated with [32P]-ATP and recombinant GST-Atg4, GST or the GST-tagged C-terminus of Atg19 (Atg19Cterm), a positive control for Atg1 phosphorylation[20]. The wild-type (WT) Atg1 complex, but not the one containing Atg1^{D211A}, phosphorylated Atg4 and Atg19Cterm but not GST alone, indicating that Atg4 could indeed be a substrate of Atg1 kinase (**Figure 1a** and **Supplementary Figure 6a**). To identify the residues involved in autophagy regulation, we individually mutated the putative phospho-acceptor serines in the different Atg1 phosphorylation consensus sites to alanine or aspartate to generate non-phosphorylable or phospho-mimicking forms of Atg4, respectively. The resulting Atg4 variants were expressed in an *atg4*Δ strain carrying Pho8Δ60 and autophagy progression was determined enzymatically[21]. Only cells expressing Atg4^{S307D} exhibited an autophagy block identical to the one in the *atg4*Δ mutant carrying an empty vector (**Figure 1b**). Interestingly, the non-phosphorylable version of the same serine, i.e., Atg4^{S307A}, could not completely bypass the autophagy impairment in *atg4*Δ cells (**Figure 1b**). These phenotypes were not due to an effect of those mutations on the protein structure because introduction of a cysteine at the same position, did not impact autophagy (**Supplementary Figure 1b**). Protein mass spectrometry analysis of Atg4$^{V297R,\ Q314K}$-GFP isolated from WT cells revealed that the peptide containing serine 307 (S307) is indeed phosphorylated in vivo (**Supplementary Figure 2a** and **Supplementary Table 2**). Atg4$^{V297R,\ Q314K}$ is a version of Atg4 where two extra trypsin cleavage sites were introduced to obtain peptides containing the region of interest detectable by protein mass spectrometry (**Supplementary Figure 2b** and **7b**). Because of the very low abundance of the phospho-peptide of interest and the presence of 3 consecutive serines, however, we could not assign with certitude a phosphorylation to S307. To precisely determine the residue modified by Atg1, we performed an in vitro kinase phosphorylation assay. We confirmed that a peptide containing the Atg1 phosphorylation consensus region around serine 307 (WT) was phosphorylated by Atg1 like the positive control peptide, i.e., GDS (**Figure 1c and Supplementary Figure 6b**). As expected, the mutant peptides S307A

and AAA were not phosphorylated (**Figure 1c** and **Supplementary Figure 6b**). We concluded that the S307 residue can be modified by Atg1.To further assess the role of S307 in autophagy, we examined by electron microscopy the presence of autophagic bodies (AB) in cells lacking the major vacuolar protease Pep4[21]. The *atg4*Δ *pep4*Δ strain expressing Atg4^{S307D} exhibited the same severe decrease in the number of AB as the one carrying protease-dead Atg4 (Atg4^{PD})[10] or an empty vector (*atg4*Δ *pep4*Δ) (**Figure 1d** and **Supplementary Figure 3a**). The very few AB observed in the vacuole lumen of this mutant have a strongly reduced size (**Figure 1d, e**). In contrast, the strain expressing Atg4^{S307A} displayed the same number of AB as the control, i.e. cells carrying Atg4 (**Figure 1d, e**). Interestingly, the average diameter of the AB in this mutant was smaller than in the control (**Figure 1f**), also explaining its slightly lower autophagy activity (**Figure 1b**) and impaired aminopeptidase 1 (Ape1) maturation (**Supplementary Figure 3b)**[22]. The similarity in phenotype shared by Atg4^{S307D} and Atg4^{PD} prompted us to analyze the proteolytic activity of the Atg4^{S307D} and Atg4^{S307A} mutants. First, we assessed the post-translational C-terminal cleavage of Atg8 by Atg4 using the Atg8-GFP chimera[8]. This analysis revealed that the Atg4^{S307D} mutant is proteolytically inactive similarly to Atg4^{PD} (**Figure 2a** and **Supplementary Figure 7a**). Atg4^{S307A}, in contrast, behaved as WT Atg4 and normally cleaved Atg8-GFP (**Figure 2a** and **Supplementary Figure7a**). Expression of GFP-Atg8ΔR in an *atg4*Δ background allows the conjugation of Atg8 to PE independently of Atg4, permitting to specifically analyze the deconjugating capacity of Atg4[15]. As reported, PE-anchored GFP-Atg8 failed to be released from the surface of autophagosomes in *atg4*Δ cells carrying either an empty vector or Atg4^{PD}, and thus the fluorescence signal was mainly detected on the vacuolar limiting membrane highlighted with the specific vacuolar membrane dye FM4-64 (**Figure 2b, c**) [15].

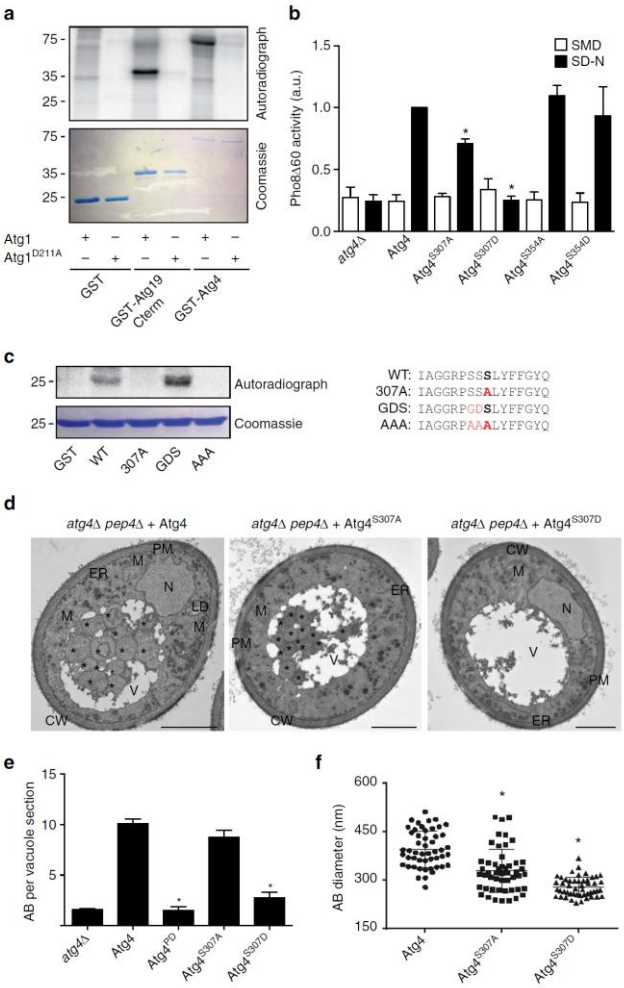

Figure 1. Atg1 phosphorylation of Atg4 inhibits autophagy. (a) GST, GST-Atg19Cterm and GST-Atg4 were expressed in *E. coli*, immobilized on beads and in vitro phosphorylated with soluble Atg1-TAP and Atg1^{D211A}-TAP complexes. The phosphorylation of the substrates was analyzed by autoradiography while their amounts were assessed by Coomassie brilliant blue staining of SDS-PAGE gels. (b) The *atg4*Δ (SAY130) strain carrying an empty pRS416 vector (*atg4*Δ) or plasmids expressing different Atg4 variants (Atg4, Atg4^{S307A}, Atg4^{S307D}, Atg4^{S354A} or Atg4^{S354D}) was grown in SMD or nitrogen starved (SD-N) for 3 h before measuring Pho8Δ60 activity in cell lysates. The symbol * indicates statistical significance ($p<0.01$) with the cells carrying Atg4 was calculated with the paired two-tailed Student's *t*'test and a.u. stands for arbitrary units. (c) GST fusions of the indicated peptides (right panel) were expressed in *E.coli* and analyzed as in (a). The amino acid in position 307 is in bold and mutated amino acids are in red. (d) The *atg4Δ pep4Δ* strain transformed with integration plasmids expressing Atg4-GFP

(SAY144), Atg4^{S307A}-GFP (JSY164) or Atg4^{S307D}-GFP (JSY165) was grown in YPD to an early log phase and then nitrogen starved in SD-N for 3 h before processing the samples for EM. Autophagic bodies (AB) are highlighted in the EM micrographs with asterisks. CW, cell wall; ER, endoplasmic reticulum; LD, Lipid droplet; M, mitochondrion; N, nucleus; PM, plasma membrane; V, vacuole. Scale bar, 1 µm. (e) Quantification of the average number of AB per vacuole section in the samples of (d). Significant differences ($p<0,0001$) between the various Atg4 mutants and the WT are indicated with the symbol * and were calculated with the paired two-tailed Student's *t*'test. (f) Determination of the average diameter of the AB in WT, Atg4^{S307A} and Atg4^{S307D} samples of (d) (n=50). Significant differences ($p<0.01$) with the WT are indicated with the symbol * and were calculated with the paired two-tailed Student's *t*'test

Complementation of the *atg4*Δ mutant with WT Atg4 led to normal Atg8 recycling and delivery of autophagosomes into the vacuolar lumen (**Figure 2b, c**)[15]. The same was observed in cells expressing Atg4^{S307A} indicating that GFP-Atg8–PE was normally processed upon autophagosome completion. In contrast, the GFP signal was mainly localized to the vacuolar rim in cells harbouring Atg4^{S307D}, revealing that this mutant is unable to recycle GFP-Atg8–PE, as observed in the Atg4^{PD} mutant (**Figure 2b, c**).The fluorescence microscopy observations about the distribution of the GFP signal were confirmed by western blot analysis, in which higher amounts of free GFP were observed in WT Atg4 and Atg4^{S307A} strains, in which GFP signal was localized inside the vacuole, indicating normal autophagy flux (**Supplementary Figure 3b, c**). To acquire more information about the dynamics of autophagosomes in presence of the different Atg4 variants, the same strains, which express GFP-Atg8ΔR and thus allow to bypass the post-translational C-terminal cleavage defect of cells expressing Atg4^{S307D} (**Figure 2a**), were examined by time-lapse microscopy. As shown in **Supplementary Figure 4** and **Supplementary Movie 1**, strain carrying WT Atg4 was slightly longer than the one reported, i.e., 11.73±0.96 min vs. 5–8 min[23], probably because cells expressing the same GFP-Atg8ΔR construct generate bigger autophagosomes[15]. **4 and Supplementary Movie 2)**. These alterations possibly lead to a reduction in the autophagic flux providing a possible explanation for its slightly lower autophagic activity (**Figure 1b**) and impaired Ape1 maturation (**Supplementary Figure 3b**) of the Atg4^{S307A} strains. The autophagosome life time in the Atg4^{S307D} mutant (8.59±2.14 min) did

not significantly differ from that in the WT (**Supplementary Fig.4** and **Supplementary Movie 3**).

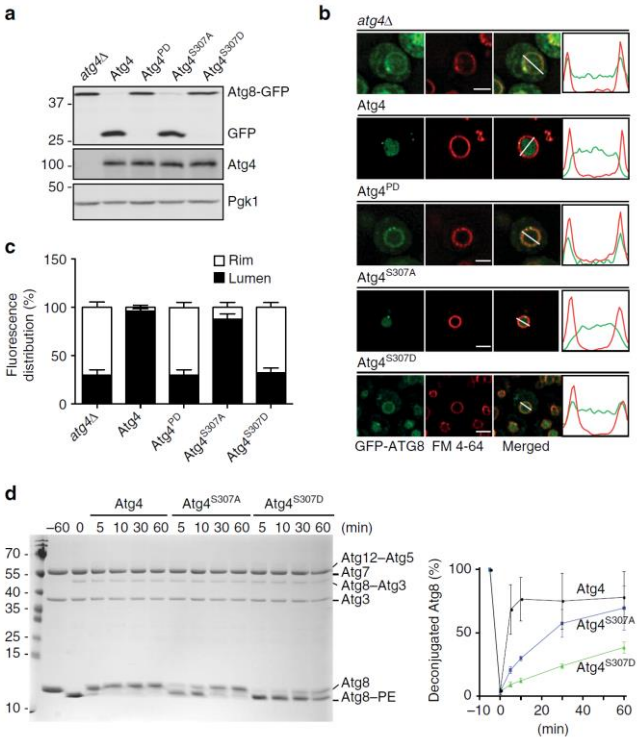

Figure 2. Atg4 phosphorylation on serine 307 blocks Atg4 function. (a) The *atg4* cells carrying the integration plasmid pCuATG8GFP(403) (SAY114) and an empt vector (*atg4*Δ) or plasmids expressing the indicated 13xmyc-tagged Atg4 varian were grown in SMD and nitrogen starved in SD-N medium for 3 h. Proteins wer precipitated with TCA and analyzed by western blot. (b) The *atg4*Δ strain carrying th integra tion plasmid pCuGFPAtg8ΔR(305) (JSY151) or plasmids expressing th indicated 13xmyc-tagged Atg4 variants were grown in SMD, nitrogen starved in SD N for 3 h, labeled with the vacuole-specific dye FM 4-64 and imaged. DIC, differenti interference contrast. Scale bar, 5 µm. Fluorescence intensity plots of representativ vacuoles are shown (indicated by white lines). (c) Quantification of GFP-Atg8Δ distribution on vacuole, i.e. rim versus lumen, in cells imaged in (a) was performed a described in Methods. Results are mean ± SD (n=50). (d) Atg8ΔR was conjugated t SUVs via the addition of Atg7, Atg3, Atg12—Atg5, $MgCl_2$ and ATP. Deconjugatic was initiated by the addition of WT Atg4 or the indicated mutants. Samples wer collected after 5, 10, 30 and 60 min, and separated on a 11% SDS gel supplemente with 4.5 M urea. The graph on the right shows the quantification of 3 independer experiments.

However, the strongly reduced size of these carriers (**Figure 1d, e**) implies that the time of autophagosome formation in Atg4^{S307D} expressing cells is a fraction of the one in the WT strain resulting in a marked reduction of the fusion events. To further demonstrate that phosphorylation of S307 modulates Atg4-mediated deconjugation of Atg8 from PE, we examined the functionality of the different Atg4 mutants *in vitro*. Atg8–PE was completely deconjugated from small unilamellar vesicles (SUVs) 10 min after the addition of Atg4 (**Figure 2d**). The deconjugation of Atg8 from PE by Atg4^{S307A} was slightly delayed compared to WT Atg4. In agreement with the *in vivo* assay, Atg4^{S307D} displayed a very severe defect in Atg8–PE processing (**Figure 2d**).

Atg4 phosphorylation affects its interaction with Atg8

Atg1 phosphorylation at S307 could inhibit Atg4 functionality by either allosterically altering the catalytic site or by interfering with the substrate binding. We first tested the Atg4–Atg8 interaction using the yeast two-hybrid (Y2H) assay. As shown in **Figure 3a**, cells exclusively expressing Atg8 did not grow on selective medium whereas those expressing both Atg4 and Atg8 displayed cell growth, confirming the interaction between these two proteins (**Figure 3a**)[24]. Noteworthy, the interaction of Atg4^{S307A} and Atg4^{PD} with Atg8 was stronger than the one detected between Atg4 and Atg8. In contrast, cells carrying Atg4^{S307D} and Atg8 did not grow on the selective medium implying that this Atg4 mutant is unable to interact with Atg8 (**Figure 3a**). The Y2H assay, however, cannot distinguish between Atg4 interaction with Atg8 or Atg8–PE. To overcome this limitation and test the binding of Atg4 variants to Atg8–PE, we performed a pull-down experiment in cells expressing GFP-Atg8ΔR. In line with the Y2H results, Atg4^{PD} and Atg4^{S307A} interaction with Atg8–PE was considerably stronger than the one observed with WT Atg4 (**Figure 3b** and **Supplementary Figure 8**). Atg4^{S307D} showed scarce binding to Atg8–PE indicating that this mutant lost almost completely its ability to interact with both Atg8 and Atg8–PE (**Figure 3b** and **Supplementary Figure 8**). Taken together, these data suggest that phosphorylation at S307 modulates the binding of Atg4 to Atg8.

Atg1 and Atg4 interact on autophagosomal membranes

Atg4 phosphorylation at S307 blocks Atg8 proteolytic processing and recycling. Hence, Atg4 must be spatially regulated to allow the initial cleavage of Atg8 essential for its conjugation to PE and also avoid a premature Atg8–PE deconjugation until autophagosome biogenesis is completed. With Atg1 being a key regulator at the PAS and Atg4 one of its substrates (**Figure 1a, c**), their interaction on autophagosomal membranes would provide a local regulation of Atg4 function.

To address this notion, we performed a bimolecular fluorescence complementation (BiFC) assay[25]. In strains expressing only the N (VN) or the C-terminal (VC) fragment of Venus fused with Atg1 and Atg4, respectively, no fluorescence signal was detected (**Supplementary Figure 3d**). BiFC signal was also absent in the strain carrying both Atg4–VC and Atg1–VN (**Figure 4a**), probably due to the transient location of Atg proteins at the PAS. In agreement with this, a perivacuolar punctuate BiFC signal became evident in an *atg2*Δ mutant in which Atg1 associates more pronouncedly to the PAS[17]. These BiFC puncta co-localized with mCherryV5-Atg8, supporting that Atg4 interacts with Atg1 at this specific location (**Figure 4a**). Additional deletion of ATG13 in this background prevents recruitment of Atg1 to the PAS[17] and led to the disappearance of BiFC signals confirming that the interaction between Atg1 and Atg4 specifically takes place on autophagosomal membranes (**Figure 4a**).

Figure 3. The phosphorylation state of S307 modulates Atg4 interaction with Atg8. (a) Atg4 and Atg8 were fused to the activation domain (AD) and/or the DNA-binding domain (BD) of Gal4, respectively. Plasmids were transformed into the PJ69-4A strain and colonies were spotted on medium lacking leucine and uracil (control plate) or leucine, uracil and adenine (test plate). Growth on the test plate indicates interaction. The control was cells expressing BD-Atg8 alone. (b) Phosphorylation of S307 blocks the interaction of Atg4 with conjugated Atg8. The *atg4*Δ (SAY084) mutant transformed with WT Atg4-13xmyc and the *atg4*Δ strain with stably integrated pCuGFPAtg8ΔR (305) (JSY151) carrying a plasmid expressing the 13xmyc-tagged WT or the indicated Atg4 variants, were exponentially grown and nitrogen starved in SD-N for 1 h. Cell lysates were subjected to pull-down experiments using GFP-trap sepharose beads. Isolated proteins, 4% of cell lysate

(input) or 100% of the pull-down material (IP), were resolved by SDS-PAGE and analyzed by western blot using anti-myc and anti-Atg8 antibodies.

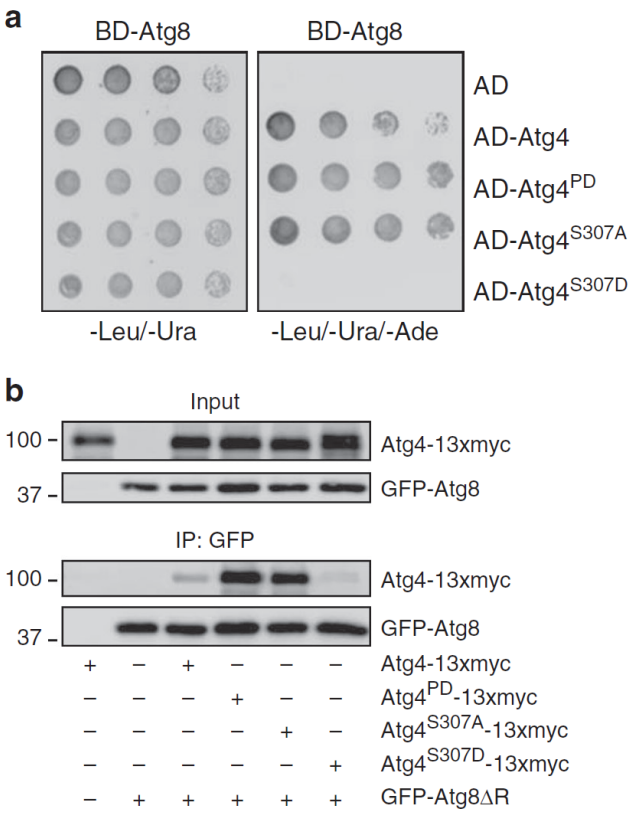

Discussion

The recruitment of Atg proteins to the PAS and their dissociation from the surface of complete autophagosomes must be subjected to spatial and temporal regulation to avoid the formation of aberrant intermediate structures. It has been shown that Atg4 constitutively deconjugates Atg8 from PE on all membranes except the PAS, suggesting the existence of regulatory elements protecting Atg8–PE from cleavage by Atg4 at this site[9]. Here, we found that active Atg1 inhibits Atg4 action at the PAS. In contrast to the rest of the Atg proteins[17], Atg4 does not localize at this location suggesting that it only very transiently associates with it[9]. As a result, a possible mechanistic model is that

Atg1 prevents Atg4 interaction with its substrate at the PAS, i.e., Atg8–PE. This transient inhibition could be one of the mechanisms that allow the synthesis and the maintenance of the Atg8–PE pool required for the formation of an autophagosome. At the completion of an autophagosome, inactivation of Atg1 would permit Atg4 to act on the Atg8–PE on autophagosomal membranes (**Figure 4b**)[11,13,15]. This hypothetical model is indirectly supported by the observation that the human homologue of Atg13, very likely in complex with Atg1/ULK1, is one of the first Atg proteins dissociating from autophagosomes when those separate from omegasomes, a step that possibly takes place at their sealing[26]. Atg1 directly inhibits Atg4 protease activity through phosphorylation of S307. The lack of interaction between $Atg4^{S307D}$ and Atg8 (**Figure 3**) indicates that this modification affects Atg4 binding to its substrate rather than negatively regulating its proteolytic activity by altering the catalytic site. This is indirectly supported by the observation that catalytically dead $Atg4^{PD}$ binds Atg8 (**Figure 3**). Nonetheless, based on the predicted Atg4 structure (**Supplementary Figure 5a**), S307 is close to amino acids D322 and H324, which correspond to D278 and H280 in ATG4B's catalytic site[27]. In particular, S307 faces H324 and when phosphorylated, its interaction with the positively charged H324 could induce a conformational change that alters the predicted Atg8-binding region (**Supplementary Figure 5a**). The interaction between phosphorylated S307 and H324, however, could also lead to a closure of the catalytic pocket.

Our multiple approaches to quantify the degree of phosphorylation of S307 in vivo have been unsuccessful probably due to the very low amounts of this modification, which make it not always detectable. This suggests that only a very small subpopulation of S307 is modified and/or is a very transient phosphorylation of S307. One possibility is that Atg4 approaching the Atg8–PE on autophagosomal membranes gets phosphorylated and, it is rapidly dephosphorylated after immediate release into the cytoplasm. Another possible scenario emerges from few recent publications. A structural study describing the mechanism of Legionella RavZ-mediated LC3–PE C-terminal processing reached the conclusion that the N-terminal and C-terminal LIR motifs in RavZ are

essential to bind the substrate simultaneously and open the catalytic groove to allow the access to the bond that has to be cleaved[28].

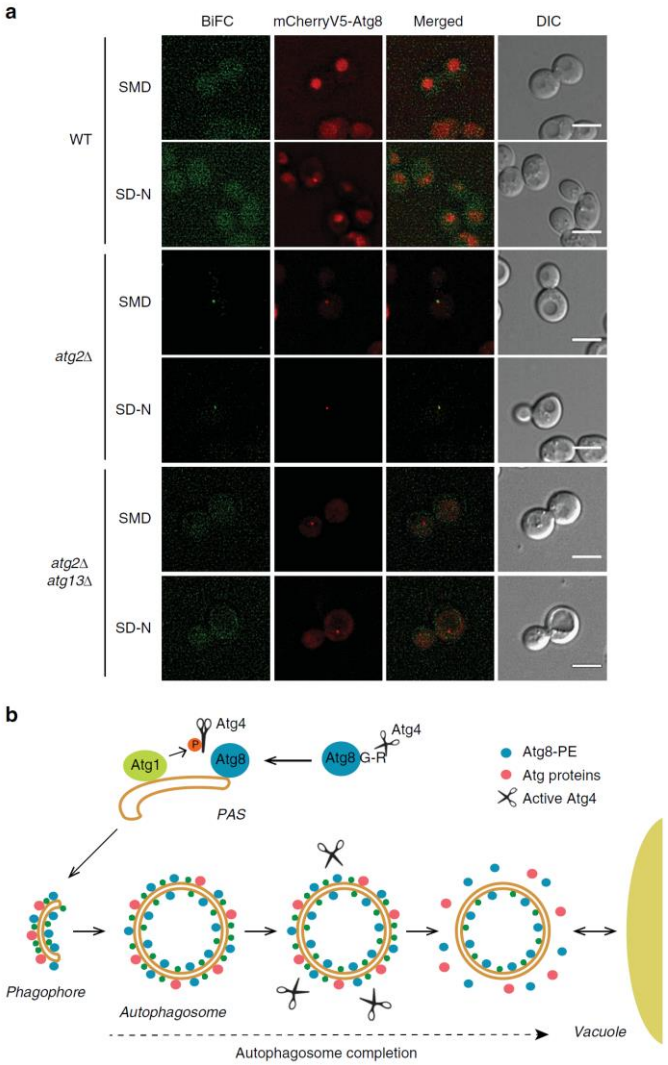

Figure 4. Atg1 and Atg4 interact at the PAS. (a) Atg1-Atg4 interaction at the PAS was visualized by BiFC. WT (JSY185), *atg2*Δ (JSY190) and *atg2*Δ *atg13*Δ (JSY215) cells expressing both endogenous Atg1-VN and Atg4-VC, and carrying a pCumCherryV5ATG8 plasmid were grown in SMD before being nitrogen starved in SD-N medium for 1 h. Fluorescence images were taken before and after nitrogen starvation. DIC, differential interference contrast. Scale bar, 5µm. (b) Mechanistic model for the regulation of Atg4 during autophagy. Newly synthesized Atg8 is constitutively processed by the cysteine protease Atg4 in the cytoplasm, where it is not inhibited by Atg1. After the cleavage of the C-terminal arginine, a glycine residue is exposed allowing Atg8 to be conjugated to the PE on autophagosomal membranes

at the PAS. During the phagophore expansion, the Atg4 adjacent or coming in proximity of autophagosomal membranes, is locally inhibited by the action of the Atg1 kinase complex Upon autophagosome completion, the release of Atg1 form autophagosomal membranes and/or its local inactivation allows Atg4 to act on Atg8-PE and release Atg8 from the PE anchor. This molecular mechanism, possibly together with other unknown regulatory events, would drive the dissociation of other Atg proteins from the surface of autophagosomes allowing their subsequent fusion with vacuoles.

LIR motifs, plus a newly identified domain, are important for the recognition and deconjugation of lapidated Atg8/LC3 proteins by Atg4 proteases in yeast and mammals[29,30]. It is thus plausible that regulation of LIR motif-mediated recruitment to autophagosomal membrane is the major mechanism for Atg8–PE processing, and Atg1 kinase inhibition represents an extra control mechanism. This latter would operate when the catalytic groove opens and therefore S307 could be of easily access for Atg1. Alignment of the amino acid sequence of Atg4 protein family members from different organisms shows that Atg4 proteins have either a serine or an alanine in the position corresponding to that of yeast S307 (**Supplementary Figure 5b**). The phylogenetic analysis reveals an evolutionary relation within Atg4 proteins with serines and within those with alanines (**Supplementary Figure 5c**). The higher Atg8–PE deconjugating activity of the Atg4 isoforms with an alanine compared to those with a serine[31,32] suggests that they might be modulated by a different and very likely, less stringent mechanism. Human ATG4B is also inhibited by ULK1 (the mammalian homologue of Atg1) through phosphorylation at S316[33]. The corresponding serine in yeast, i.e., S354, however, shows no major defect in autophagy progression when mutated to aspartate or alanine (**Figure 1b**). Interestingly, the residue equivalent to S307 of yeast Atg4 is substituted by an alanine in ATG4B (**Supplementary Figure 5b**). Altogether these observations reveal that although phosphorylation by Atg1 homologues is an evolutionary conserved mechanism to negatively regulate Atg4, different serine residues are used. Future studies are needed to decipher the significance of this difference.

Methods

Plasmids

The pATG4GFP(416) plasmid was generated by PCR amplification of *ATG4* promoter and the *ATG4-GFP* fusion from the MNY006 strain genome, and its subsequent cloning into the pRS416 vector[33] as a *Kpn*I/*Asc*I fragment. The pATG413xmyc(416) plasmid was obtained by replacing *GFP* in pATG4GFP(416) with the sequence for the 13xmyc tag from the pFA6a13xmycTRP1 plasmid[34] using *Pac*I and *Asc*I. Protease-dead (C147S), the cysteine mutant (S307C) and phospho-mutant versions of Atg4 were created by inserting nucleotide changes in the pATG4GFP(416) and pATG413xmyc(416) plasmids using the site-direct mutagenesis kit (Stratagene, LaJolla, CA). The correct introduction of the point mutations was verified by DNA sequencing. The pRS416 plasmid backbone was replaced with the one of the pRS406[33] using *Kpn*I and *Sac*I, to create the vectors integrating the various *ATG4-GFP* constructs into the genome. The integrative vectors expressing untagged Atg4, Atg4^{S307A} and Atg4^{S307D} under the control of their own promotor (i.e pATG4(406), pATG4^{S307A}(406) and pATG4^{S307D}(406) were obtained by cloning PCR products from the appropriate template plasmids as *Kpn*I-*Asc*I fragments into pATG4GFP(406), a strategy that allows to remove *GFP*. The pTEFATG4$^{V297R,\ Q314K}$-GFP(416) plasmid was generated by triple ligation into the pRS416 vector digested with *Kpn*I and *Xma*I, of a fragments carrying the *TEF1* promoter (digested with *Kpn*I and *Pac*I) and the Atg4^{V297R,Q314K} ORF (digested with *Pac*I and *Xma*I). The sequence coding for Atg4^{V297R,Q314K} was obtained beforehand by site-directed mutagenesis of the pATG4GFP(416) construct. These two-point mutations, which do not affect the functionality of Atg4 (Supplementary Fig. 2b), were introduced to add new trypsination sites in order to generate a peptide of the region of interest detectable by protein mass spectrometry analysis. The pCuGFPATG8ΔR(305) and pCuATG8GFP(403) plasmids were generated by replacing the vector backbone of the pCuGFPATG8ΔR(406)[15] and pAUT7GFP(416)

plasmid[8] with the one from the pRS305 and pRS403 vectors[33], respectively, using *Sac*I and *Xho*I. The yeast two-hybrid plasmids were created by amplifying the ORF of *ATG4* and its variants by PCR from the pATG413xmyc plasmids described above, and cloning them as a *XmaI/SalI* fragment into the pGAD-C1 vector[35]. The pGBDU-Atg8 plasmid was described elsewhere[36]. To create the plasmids expressing GST-tagged Atg4 peptides, complementary primers encoding for the peptides and containing the overhanging ends generating *EcoR*I and *Xho*I restriction sites, were annealed together to create the insert and cloned into pGEX4T3 vector as *EcoRI/Xho*I fragments. The pCumCherryV5ATG8 construct has been described elsewhere[37].

Yeast strains

The *S. cerevisiae* strains used in this study are listed in Supplementary Table 1. For gene disruptions, the coding regions were replaced with *K. lactis URA3* or *LEU2*, the *S. cerevisiae TRP1*, the *S. pombe HIS5* or the *K. pneumoniae hphNT1*gene by homologous recombination using PCR products generated with primers containing 60 bases of identity to the regions flanking the open reading frames[34,38,39]. Chromosomal tagging of the *ATG1* or *ATG4* genes at the 3'end was done by PCR-based integration of the N- or the C-terminus of the Venus tag using pFA6a-VN-His3MX6 and pFA6a-VC-TRP1 as template plasmids, respectively[25]. PCR verification, western blotting using antibodies recognizing the tags and analysis of Ape1 processing were used to confirm all deletions and integrations as well as the functionality of all the protein fusions.

Media

Yeast cells were grown in rich (YPD; 1% yeast extract, 2% peptone, and 2% glucose) or synthetic minimal (SMD; 0.67% yeast nitrogen base, 2% glucose, and amino acids and vitamins as needed) medium. Autophagy was induced by transferring cells into a nitrogen starvation medium (SD-N; 0.17% yeast nitrogen base without amino acids and ammonium sulfate, and 2% glucose) during 1 and 3 h.

Antibodies and reagents

Primary antibodies or sera for protein or tag detection were: anti-GFP antibody (Roche, cat# 11814460001, 1:3,000 dilution), anti-myc antibody (Santa Cruz, cat# sc-40, 1:10,000 dilution), anti-Ape1 antibody (1:3,000 dilution)[37] and anti-Atg8 (1:5,000 dilution)[30]. The anti-Pgk1 antiserum was generated by immunization of New Zealand White rabbits with the CLKYFGKALENPTR peptide (New England Peptides) and used at a 1:1,000 dilution. Alexa-680 conjugated anti-rabbit or mouse IgG antibodies were used as secondary antibodies (Life technologies, 1:5,000 dilution).

Fluorescence microscopy

Fluorescence signals were visualized with a DeltaVision RT fluorescence microscope (Applied Precision) equipped with a CoolSNAP HQ camera (Photometrix). Images were generated by collecting a stack of 20 pictures with focal planes 0.2 μm apart in order to cover the entire volume of a yeast cell and by successively deconvolving them using the SoftWoRx software (Applied Precision). A single focal plane is shown at each time point. The FM 4-64 dye (Invitrogen) was used to specifically stain the vacuolar rim[40]. The GFP intensity in vacuolar rim or lumen was determine as an average of the intensity of several points in each region by using the multi-point tool in ImageJ. For time-lapse imaging experiments, cells nitrogen starved in SD-N medium and stained with the CellTracker™ Blue 7-amino-4-chloromethylcoumarin (CMAC) dye (Invitrogen) for 30 min, were imaged every 30 s, collecting a Z-stack of 6 pictures with focal planes 0.30 μm apart. Images were deconvolved and mounted into movies before measuring the life of GFP-Atg8ΔR using the SoftWoRx software. The time point at which GFP-Atg8ΔR appeared as a punctuate structure was considered as time 0 min. 2D projections of Z-stack images were employed to quantify the relative intensity of GFP-Atg8ΔR-positive structures as previously described[23] and setting to 1 the relative intensity of cells expressing WT Atg4.

Yeast two-hybrid assay

The plasmids pGBDU-C1 and pGAD-C1 carrying *ATG8* and *ATG4* or its mutated forms, respectively, were transformed into the PJ69-4A test strain and grown on SMD medium lacking leucine and uracil[35]. Colonies were then spotted on SMD medium lacking leucine and uracil (control plate) or leucine, uracil and adenine (test plate).

Immunoprecipitations

The equivalent of 100 OD_{600} growing cells was transferred to SD-N medium for 1 h, harvested by centrifugation and resuspended in 1 ml of lysis buffer (45 mM HEPES, pH 7.4, 150 mM NaCl, 1 mM EDTA, 10% glycerol, 0.5% Tween-20) supplemented with 1 mM PMSF, Complete protease inhibitors (Roche), 10 mM β-glycerophosphate, 50 mM NaF and 1 mM Na_3VO_4. After addition of glass beads, cells were lysed by vortexing at 4˚C for 15 min and lysates cleared by centrifugation at 15,000 g for 5 min at 4˚C. The supernatant was incubated with 25 µl of pre-washed GFP-trap sepharose beads (ChromoTek) on a rotating wheel for 1.5 h at 4˚C. Beads were finally washed 3 times in 1 ml of lysis buffer, resuspended in loading buffer and analyzed by SDS-PAGE followed by western blot.

Electron microscopy

Fifteen OD_{600} unit equivalents of cells were resuspended in 1 ml of freshly prepared ice-cold 1.5% KMnO4 (Sigma) and transferred into a 1.5 ml microfuge tube. After topping up the tube with 0.5 ml of the same solution to exclude air, samples were mixed on a rotatory wheel for 30 min at 4˚C. This operation was repeated once more before washing the pellets five times with 1 ml of distilled water. Cells were then dehydrated in increasing amounts of acetone (10, 30, 50, 70, 90, 95 and three times 100%) by incubation on a rotatory wheel for at least 20 min at room temperature, at each step. After centrifugation, pellets were resuspended in 33% Spurr's resin in acetone and mixed on the same device for 1 h at room temperature. This operation was repeated twice overnight and successively during all day in 100% Spurr's resin.

The Spurr's resin mixture was prepared by mixing 10 g of 4-vinylcyclohexene dioxide (or ERL4206), 4 g of epichlorohydrin-polyglycol epoxy (DER) resin 736, 26 g of (2-nonen-1-yl)succinic anhydride (NSA) and 0.4 g of N,Ndiethylethanolamine (all from Sigma). Incubating the preparations overnight at 70˚C polymerized the Spurr's resin. Section of about 65–80 nm were then cut using an Ultracut E ultramicrotome (Leica Microsystems) and transferred on Formvar carbon-coated copper grids. Sections where then stained first with 6% uranyl acetate for 30 min at room temperature and then with a lead-citrate solution (80 mM lead nitrate, 120 mM sodium citrate, pH 12) for 2 min before being viewed[41]. To determine the number of AB per vacuole and their diameter, 3 different grids with sections obtained from the same preparation were evaluated. For every grid, the number and diameter of AB in 50 cells with apparent vacuoles was determined. Error bars represent the standard deviation from the counting of the 3 grids.

Protein expression and purification

Atg3, Atg4, Atg4 mutants, Atg7, Atg8 and the Atg12–Atg5 complex were expressed and purified *E. coli* Rosetta pLySS cells as described. Full length Atg3 and Atg19Cterm were expressed as N-terminal GST fusion proteins from pGEX4T1[42]. Cells were grown at 37˚C to an OD_{600} of 0.8, induced with 50 μM isopropyl β-D-1-thiogalactopyranoside (IPTG) and grown for a further 16 h at 18°C. Cells were pelleted and resuspended in a buffer containing 50 mM HEPES, pH 7.5, 300 mM NaCl, 2 mM $MgCl_2$, 1 mM DTT and Complete protease inhibitors (Roche) and DNAse I (Sigma). Cells were lysed by freeze thawing and the lysate was centrifuged at 40,000 rpm (Beckman Ti45 rotor) for 40 min at 4˚C. The supernatant was incubated with glutathione-beads (GE Healthcare) for 2h at 4˚C. Beads were washed 5 times with 50 mM HEPES, pH 7.5, 300 mM NaCl and 1 mM DTT, followed by 2 washes with 50 mM HEPES, pH 7.5, 1000 mM NaCl, 1mM DTT and two washes with 50 mM HEPES, pH 7.5, 300 mM NaCl and 1 mM DTT. The proteins were cleaved off from the GST tag by incubation with thrombin protease (Serva) overnight at 4˚C. The supernatant containing

the cleaved off Atg3 and Atg19Cterm were diluted to reach a final salt concentration of 150 mM NaCl and further purified using a 16/60 Q-Sepharose column. The protein was eluted on a gradient ranging from 150 mM-1 M NaCl. Fractions containing Atg3 and Atg19Cterm were pooled, concentrated and run on a 16/60 S75 size exclusion column in 50 mM HEPES, pH 7.5, 150mM NaCl and 1 mM DTT. Full length Atg7 was expressed as an N-terminal 6xhistidine-tagged protein from pOPTHrsTEV[42]. Cells were grown at 37°C to an OD_{600} of 0.8, induced with 50 μM IPTG and grown for a further 16 h at 18˚C. Cells were pelleted and resuspended in a buffer containing 50 mM HEPES, pH 7.5, 300 mM NaCl, 10 mM imidazole, 1 mM $MgCl_2$, 2 mM β-mercaptoethanol, Complete protease inhibitors (Roche) and DNAse I (Sigma). Cells were lysed by freeze thawing and the lysate was centrifuged at 40,000 rpm (Beckman Ti45 rotor) for 40 min at 4˚C. The supernatant was incubated with nickel beads (5 Prime) for 2 h at 4°C. Beads were washed with 50 mM HEPES, pH 7.5, 300 mM NaCl, 10 mM imidazole and 2 mM β-mercaptoethanol, and the 6xhistidine-tag was cleaved off with TEV protease at room temperature. The Atg7 protein was diluted to reach a final salt concentration of 150 mM and further purified on 16/60 Q-Sepharose column. The protein was eluted using a gradient reaching from 150 mM-1 M NaCl. Fractions containing Atg7 were pooled, concentrated and run on a 16/60 S200 size exclusion column in 50mM HEPES pH 7.5, 150mM NaCl and 1 mM DTT. Atg8 lacking the C-terminal arginine (R117, Atg8ΔR) was expressed as N-terminal 6xhistidine-tagged protein from pOPC-His-TEV-Atg8[42]. Cells were grown at 37˚C to an OD_{600} of 0.8, induced with 500 μM IPTG and grown for a further 3 h at 37˚C. Cells were pelleted and resuspended in a buffer containing 50 mM HEPES, pH 7.5, 300mM NaCl, 10 mM imidazole, 1 mM $MgCl_2$, 2 mM β−mercaptoethanol, Complete protease inhibitors (Roche) and DNAse I (Sigma). Cells were lysed by freeze thawing and the lysate was centrifuged at 40,000 rpm (Beckman Ti45 rotor) for 40 min at 4˚C. The supernatant was incubated with nickel beads (5 Prime) for 2h at 4˚C. Beads were washed with 50 mM HEPES, pH 7.5, 300 mM NaCl, 10 mM imidazole and 2 mM β−mercaptoethanol, and the 10xhistidine-tag was cleaved off for

several hours with TEV protease at room temperature. The Atg8 protein was diluted to reach final salt concentration of 150 mM and the protein was further purified on 16/60 SP-Sepharose column. The protein was eluted using a gradient reaching from 150-1000 mM NaCl. Fractions containing Atg8 were pooled, concentrated and run on a 16/60 Superdex S75 size exclusion column in 50 mM HEPES pH 7.5, 150 mM NaCl and 1mM DTT. The Atg5-Atg12 conjugate was produced by co-expression of 6xhistidine-tagged Atg5, Atg12, Atg10 and Atg7[42]. Cells were grown at 37˚C to an OD_{600} of 0.8, induced with 1mM IPTG and grown for another 4 h at 37°C. Harvested cells were resuspended in the resuspension buffer (300 mM NaCl, 5 0mM HEPES, pH 7.5, 10 mM imidazole, 2.5 mM Pefablock (Roth), 1 mM $MgCl_2$, 2 mM β-mercaptoethanol and and DNAse I (Sigma), and disrupted by freeze-thaw method and sonication. The cleared lysate was applied to a HisTrap column (GE Healthcare) and the proteins were eluted by a step-wise imidazole gradient. The Atg5-Atg12 the eluate was concentrated using Amicon Ultra centrifugal filter (MW cut-off 30 kDa) and further purified using a 16/60 S200 size exclusion column (GE Healthcare). The protein complex was eluted from the column with 150 mM NaCl, 50 mM HEPES, pH 7.5 and 1 mM DTT. Atg4 and its mutant versions were expressed as an N-terminal GST fusion protein. Cells were grown at 37˚C until an OD_{600} of 0.8. Protein expression was induced by addition of IPTG to a final concentration of 0.1 mM and the protein was expressed at 18˚C overnight. The cell pellets were resuspended in 50 mM HEPES/KOH, pH 7.5, 300 mM NaCl, 1 mM DTT, 1 mM $MgCl_2$, DNase I, Complete protease inhibitors (Roche) and PEFABLOC. Cells were lysed by freezing in liquid nitrogen and thawing, followed by brief sonication. The lysate was cleared by centrifugation at 200,000 g for 40 min at 4˚C and the supernatant was incubated with equilibrated glutathione beads (GE Healthcare) for 2 h at 4˚C. The beads were washed 5 times with 50 mM HEPES/KOH, pH 7.5, 300 mM NaCl, 1 mM DTT, 2 times with 50 mM HEPES, pH 7.5, 700 mM NaCl, 1 mM DTT and finally 2 times with 50 mM HEPES, pH 7.5, 300 mM NaCl, 1 mM DTT. The protein was eluted with 50 mM HEPES, pH 7.5, 300 mM NaCl and 1mM DTT supplemented with 20 mM L-glutathione and

cleaved with thrombin. The cleaved protein was run on a Superdex 200 16/600 column (GE Healthcare) and the peak fractions containing Atg4 were pooled, concentrated and flash frozen in liquid nitrogen.

Preparation of small unilamellar vesicles (SUVs)

SUVs used for the conjugation and deconjugation assays were composed of 65% DOPC, 30% DOPE and 5% PI (all purchased from Avanti Polar Lipids). 100 µl of the lipid stock (10 mg/ml) were transferred into a glass vial and dried under an argon stream. The dried lipids were dried additionally for 1 h in a desiccator. Subsequently, the dried lipids were subsequently incubated with SUV buffer (25 mM HEPES, pH 7.5, 137 mM NaCl, 2.7 mM KCl, 1 mM DTT) for 15 min. The lipids were resuspended by tapping and gently sonicated for 2 min in a water bath sonicator. The resuspended SUVs were then extruded 21 times through a 0.4 µm membrane followed by extrusion through a 0.1 µm membrane (Whatman Nucleopore, St. Louis, MO) using the Mini Extruder (Avanti Polar Lipids). The final SUVs suspension has a concentration of 1 mg lipids/ml buffer.

Atg8 conjugation and deconjugation assay using SUVs

The conjugation and deconjugation reactions were performed at 30˚C and all buffers, solutions and the SUVs with the exception of the proteins were pre-warmed to this temperature. Atg3 and Atg7 were used at a final concentration of 1 µM, whereas Atg12–Atg5 and Atg8ΔR were used at a final concentration of 0.5 µM and 5 µM, respectively. ATP was added to a final concentration of 50 µM while $MgCl_2$ was used at 1 mM. Conjugation reactions were stopped by the addition of 1000 units of calf intestinal phosphatase (New England Biolabs). For the deconjugation reaction, Atg4 was used at a final concentration of 25 nM. The reactions were then stopped by the addition of SDS-PAGE loading buffer and samples separated on 11% SDS- PAGE gels containing 4.5 M urea in the separating part.

Protein mass spectrometry analysis

700 ml of late stationary grown *atg4*Δ cells (SAY084) transformed with the pTEFATG4$^{V297R,\ Q314K}$-GFP(416) plasmid and nitrogen starved in SD-N medium for 1 h were lysed by cryogenic grinding in 45 mM HEPES, pH 7.4, 150 mM NaCl, 1 mM EDTA, 10% glycerol, 0.5% Tween-20 supplemented with 1 mM PMSF, Complete protease inhibitors (Roche), 10 mM β-glycerophosphate, 10 mM NaF and 1 mM Na_3VO_4 buffer. Lysates were then cleared by centrifugation and incubated with 100 µl GFP-sepharose beads. Immuno-isolated Atg4$^{V297R,\ Q314K}$-GFP was eluted in sample buffer and separated by SDS-PAGE before cutting the gel band containing the fusion protein. After in-gel trypsination, the resulting peptides were separated and analyzed by liquid chromatography-mass spectrometry (LC-MS) on a Q-Exactive plus MS instrument with an Ultimate 3000 nano RSLC LC system (Thermo). Peptides were fragmented by collision-induced dissociation, and the resulting peptide MS/MS spectra were used for identification of proteins and modifications, performed with the PEAKS software version 7.5 (Bioinformatics Solutions).

In vitro Atg1 phosphorylation

Atg1-TAP and Atg1^{D211A}-TAP, and the associated proteins, were immunoisolated from yeast grown in 2 l of YPD medium to an OD_{600} of 2 and treated with 220 nM rapamycin for 1 h, harvested by centrifugation, and washed in PBS, 2% glucose. Cells were then resuspended in the lysis buffer (PBS, 10% glycerol, 0.5% Tween-20, 1 mM NaF, 1 mM phenylmethylsulfonylfluoride, 1 mM Na_3VO_4, 20 mM β-glycerophosphate, protease inhibitor cocktail (Roche)) and frozen in droplets in liquid nitrogen. After cell disruption with a freezer mill (6770; SPEX), the extract was thawed in lysis buffer and cleared by centrifugation. The cleared extracts were then incubated with 160 µl of IgG-coupled magnetic beads (Dynabeads, Invitrogen) for 1 h at 4°C with rotation. The beads were washed six times for 5–10 min in lysis buffer with rotation and cleaved in lysis buffer containing 0.5 mM DTT and the TEV protease for 1 h at 16°C with slow shaking. The immunoisolated Atg1-TAP and Atg1^{D211A}-TAP, and the associated proteins, were incubated in the phosphorylation mixture (10 µCi γATP,

25 mM MOPS pH 7.5, 1 mM EGTA, 10 mM Na_3VO_4, 15 mM $MgCl_2$ total volume of 11 µl) with 2 µg of soluble GST, GST-Atg19Cterm or GST-Atg4, purified from *E. coli*[20]. After 20 min of incubation at 30˚C, the Atg1 bound beads were removed and the supernatant was assessed for radioactivity incorporation by phospho-imaging. GST-fused peptides were immobilized on GST beads and TEV eluted soluble Atg1 complexes were used for the *in vitro* phosphorylation reaction as described above.

Pho8Δ60 assay

As previously described[21], 5 OD_{600} equivalents of cells were lysed in 400 µl of ice-cold lysis buffer (20 mM PIPES, pH 6.8, 0.5% Triton X-100, 50 mM KCl, 100 mM potassium acetate, 10 mM $MgCl_2$, 10 µM $ZnSO_4$, 2 mM PMSF) by vortexing in presence of 100 µl of glass beads (0.4-0.6 mm in diameter) for 3–5 min at 4˚C. Lysates were centrifuged at 13,000 g for 5 min at 4˚C. Then 100 µl of supernatant were mixed with 400 µl of ALP reaction buffer (250 mM Tris-HCl, pH 8.5, 0.4% Triton X-100, 10 mM $MgCl_2$, 10 µM $ZnSO_4$, 1.25 mM *p*-nitrophenyl phosphate) pre-warmed at 37˚C. Samples were incubated at 37˚C for 20 min before adding 500 µl of 1 M glycine, pH 11.0. After centrifuge at 13,000 g for 2 min, the absorbance of the supernatant was measured at 400 nm. Enzymatic activity was calculated with the following formula 1000 x OD_{400}/ [time x protein concentration in µg/ml] and expressed in arbitrary units.

Western blot analyses

Western blot analyses were conducted as previously described[21]. Briefly, 2.5 OD_{600} equivalents of cells were collected by centrifugation at 13,000 g for 1 min and resuspended in 400 µl of ice-cold 10% trichloroacetic acid (TCA). After having left them on ice for at least 30 min, mixtures were centrifuged at 13,000 g for 5 min at 4°C and the protein pellets were resuspended in 1 ml of ice-cold acetone by sonication. Samples were subsequently put at -20°C for at least 20 min before to be centrifuged at 13,000 g for 5 min at 4°C. Pellets were dried, resuspended in 80-100 µl of 1x Laemmli sample buffer (50 mM Tris-

HCl, pH 6.8, 2% SDS, 10% glycerol, 1% β-mercaptoethanol) and boiled before to be loaded on SDS-PAGE gels. Protein were finally transferred on PVDF membranes and detected using an Odyssey system (Li Cor Biosciences) and ImageJ software was used for processing of images and band quantification.

Statistical analyses

Statistical analyses were done using the paired two-tailed Student's *t*-test.

Acknowledgements

The authors thank Daniel Klionsky for reagents. We also thank Hjalmar Permentier, Marcel de Vries and Margot Jeronimus-Stratingh of the Interfaculty Mass Spectrometry Center (University of Groningen/University Medical Center Groningen) for the mass spectrometry analyses, and Klaas Sjollema of the UMCG Microscopy & Imaging Center. F.R. is supported by ALW Open Program (822.02.014), DFG-NWO cooperation (DN82-303), SNF Sinergia (CRSII3_154421) and ZonMW VICI (016.130.606) grants. S.M. is supported by (FP7/2007-2013)/ERC grant agreement No. 260304, the FWF Austrian Science Fund (grant number P25546-B20) and the EMBO Young Investigator Program. C.K. is supported by a grant from the Vienna Science and Technology Fund (WWTF, VRG10-001) the Austrian Science Fund (FWF, P 25522-B20 and P 28113-B28) and the EMBO Young Investigator Program. C.U. is supported by the DFG (UN111/7-2) and the Hans-Mühlenhoff foundation. R.G.-S. is supported by a Marie Sklodowska-Curie Individual Fellowship (IF-EF) from the European Commission. S.A. is a recipient of the FCT grant SFRH/BD/95013/2013.

References

1. Choi, A. M. K., Ryter, S. W. & Levine, B. Autophagy in Human Health and Disease. *N. Engl. J. Med.* **368,** 651–662 (2013).
2. Reggiori, F. & Klionsky, D. J. Autophagic Processes in Yeast: Mechanism, Machinery and Regulation. **194,** 341–361 (2013).
3. Noda, N. N. & Fujioka, Y. Atg1 family kinases in autophagy initiation. *Cell. Mol. Life Sci.* **72,** 3083–96 (2015).

4. Ganley, I. G. Autophagosome maturation and lysosomal fusion. *Essays Biochem.* **55,** 65–78 (2013).
5. Cebollero, E. *et al.* Phosphatidylinositol-3-phosphate clearance plays a key role in autophagosome completion. *Curr. Biol.* **22,** 1545–1553 (2012).
6. Cheng, J. *et al.* Yeast and mammalian autophagosomes exhibit distinct phosphatidylinositol 3-phosphate asymmetries. *Nat. Commun.* **5,** 1–10 (2014).
7. Nair, U., Cao, Y., Xie, Z. & Klionsky, D. J. Roles of the Lipid-binding Motifs of Atg18 and Atg21 in the Cytoplasm to Vacuole Targeting Pathway and Autophagy. *J. Biol. Chem.* **285,** 11476–11488 (2010).
8. Kim, J., Huang, W. P. & Klionsky, D. J. Membrane recruitment of Aut7p in the autophagy and cytoplasm to vacuole targeting pathways requires Aut1p, Aut2p, and the autophagy conjugation complex. *J. Cell Biol.* **152,** 51–64 (2001).
9. Nakatogawa, H., Ishii, J., Asai, E. & Ohsumi, Y. Atg4 recycles inappropriately lipidated Atg8 to promote autophagosome biogenesis. *Autophagy* **8,** 177–186 (2012).
10. Kirisako, T. *et al.* The reversible modification regulates the membrane-binding state of Apg8/Aut7 essential for autophagy and the cytoplasm to vacuole targeting pathway. *J. Cell Biol.* **151,** 263–275 (2000).
11. Nakatogawa, H., Ichimura, Y. & Ohsumi, Y. Atg8, a ubiquitin-like protein required for autophagosome formation, mediates membrane tethering and hemifusion. *Cell* **130,** 165–178 (2007).
12. Xie, Z., Nair, U. & Klionsky, D. J. Atg8 Controls Phagophore Expansion during Autophagosome Formation. *Mol. Biol. Cell* **19,** 3290–3298 (2008).
13. Kaufmann, A., Beier, V., Franquelim, H. G. & Wollert, T. Molecular mechanism of autophagic membrane-scaffold assembly and disassembly. *Cell* **156,** 469–481 (2014).
14. Tanida, I. *et al.* HsAtg4B/HsApg4B/autophagin-1 cleaves the carboxyl termini of three human Atg8 homologues and delipidates microtubule-associated protein light chain 3- and GABAA receptor-associated protein-phospholipid conjugates. *J. Biol. Chem.* **279,** 36268–36276 (2004).
15. Nair, U. *et al.* A role for Atg8-PE deconjugation in autophagosome biogenesis. *Autophagy* **8,** 780–793 (2012).
16. Yu, Z.-Q. *et al.* Dual roles of Atg8−PE deconjugation by Atg4 in autophagy. *Autophagy* **8,** 877–876 (2012).
17. Suzuki, K., Kubota, Y., Sekito, T. & Ohsumi, Y. Hierarchy of Atg proteins in pre-autophagosomal structure organization. *Genes to Cells* **12,** 209–218 (2007).
18. Ogura, K. i. *et al.* Protein phosphatase 2A cooperates with the autophagy-related kinase UNC-51 to regulate axon guidance in Caenorhabditis elegans. *Development* **137,** 1657–1667 (2010).
19. Papinski, D. *et al.* Early steps in autophagy depend on direct phosphorylation of Atg9 by the Atg1 kinase. *Mol. Cell* **53,** 471–483 (2014).

20. Pfaffenwimmer, T. *et al.* Hrr25 kinase promotes selective autophagy by phosphorylating the cargo receptor Atg19. *EMBO Rep.* **15,** 862–70 (2014).
21. Guimaraes, R. S., Delorme-Axford, E., Klionsky, D. J. & Reggiori, F. Assays for the biochemical and ultrastructural measurement of selective and nonselective types of autophagy in the yeast Saccharomyces cerevisiae. *Methods* **75,** 141–150 (2015).
22. Shintani, T., Huang, W. P., Stromhaug, P. E. & Klionsky, D. J. Mechanism of cargo selection in the cytoplasm to vacuole targeting pathway. *Dev. Cell* **3,** 825–837 (2002).
23. Geng, J., Baba, M., Nair, U. & Klionsky, D. J. Quantitative analysis of autophagy-related protein stoichiometry by fluorescence microscopy. *J. Cell Biol.* (2008). doi:10.1083/jcb.200711112
24. Lang, T. *et al.* Aut2p and Aut7p, two novel microtubule-associated proteins are essential for delivery of autophagic vesicles to the vacuole. *EMBO J.* **17,** 3597–3607 (1998).
25. Sung, M.-K. & Huh, W.-K. Bimolecular fluorescence complementation analysis system forin vivo detection of protein–protein interaction inSaccharomyces cerevisiae. *Yeast* **24,** 767–775 (2007).
26. Karanasios, E. *et al.* Dynamic association of the ULK1 complex with omegasomes during autophagy induction. *J. Cell Sci.* **126,** 5224–5238 (2013).
27. Satoo, K. *et al.* The structure of Atg4B-LC3 complex reveals the mechanism of LC3 processing and delipidation during autophagy. *EMBO J.* **28,** 1341–1350 (2009).
28. Kwon, D. H. *et al.* The 1:2 complex between RavZ and LC3 reveals a mechanism for deconjugation of LC3 on the phagophore membrane. *Autophagy* **13,** 70–81 (2017).
29. Skytte Rasmussen, M. *et al.* ATG4B contains a C-terminal LIR motif important for binding and efficient cleavage of mammalian orthologs of yeast Atg8. *Autophagy* **13,** 834–853 (2017).
30. Abreu, S. *et al.* Conserved Atg8 recognition sites mediate Atg4 association with autophagosomal membranes and Atg8 deconjugation. *EMBO Rep.* **18,** 765–780 (2017).
31. Li, M. *et al.* Kinetics comparisons of mammalian Atg4 homologues indicate selective preferences toward diverse Atg8 substrates. *J. Biol. Chem.* **286,** 7327–7338 (2011).
32. Wu, F., Li, Y., Wang, F., Noda, N. N. & Zhang, H. Differential Function of the Two Atg4 Homologues in the Aggrephagy Pathway in *Caenorhabditis elegans*. *J. Biol. Chem.* **287,** 29457–29467 (2012).
33. Sikorski, R. S. & Hieter, P. A system of shuttle vectors and yeast host strains designed for efficient manipulation of DNA in Saccharomyces cerevisiae. *Genetics* **122,** 19–27 (1989).
34. Longtine, M. S. *et al.* Additional modules for versatile and economical PCR-based gene deletion and modification in Saccharomyces cerevisiae.

Yeast **14,** 953–961 (1998).
35. James, P., Halladay, J. & Craig, E. A. Genomic libraries and a host strain designed for highly efficient two-hybrid selection in yeast. *Genetics* **144,** 1425–36 (1996).
36. Strømhaug, P. E., Reggiori, F., Guan, J., Wang, C.-W. & Klionsky, D. J. Atg21 Is a Phosphoinositide Binding Protein Required for Efficient Lipidation and Localization of Atg8 during Uptake of Aminopeptidase I by Selective Autophagy. *Mol. Biol. Cell* **15,** 3553–3566 (2004).
37. Mari, M. *et al.* An Atg9-containing compartment that functions in the early steps of autophagosome biogenesis. *J. Cell Biol.* **190,** 1005–1022 (2010).
38. Gueldener, U., Heinisch, J., Koehler, G. J., Voss, D. & Hegemann, J. H. A second set of loxP marker cassettes for Cre-mediated multiple gene knockouts in budding yeast. *Nucleic Acids Res.* **30,** e23 (2002).
39. Janke, C. *et al.* A versatile toolbox for PCR-based tagging of yeast genes: new fluorescent proteins, more markers and promoter substitution cassettes. *Yeast* **21,** 947–962 (2004).
40. Vida, T. A. & Emr, S. D. A new vital stain for visualizing vacuolar membrane dynamics and endocytosis in yeast. *J. Cell Biol.* **128,** 779–92 (1995).
41. Griffith, J., Mari, M., De Mazière, A. & Reggiori, F. A Cryosectioning Procedure for the Ultrastructural Analysis and the Immunogold Labelling of Yeast Saccharomyces cerevisiae. *Traffic* **9,** 1060–1072 (2008).
42. Romanov, J. *et al.* Mechanism and functions of membrane binding by the Atg5-Atg12/Atg16 complex during autophagosome formation. *EMBO J.* **31,** 4304–4317 (2012).
43. Robinson, J. S., Klionsky, D. J., Banta, L. M. & Emr, S. D. Protein sorting in Saccharomyces cerevisiae: isolation of mutants defective in the delivery and processing of multiple vacuolar hydrolases. *Mol. Cell. Biol.* **8,** 4936–48 (1988).
44. Noda, T., Matsuura, A., Wada, Y. & Ohsumi, Y. Novel System for Monitoring Autophagy in the Yeast Saccharomyces cerevisiae. *Biochem. Biophys. Res. Commun.* **210,** 126–132 (1995).

Supplementary figures

a

```
  1 MQRWLQLWKM DLVQKVSHGV FEGSSEEPAA LMNHDYIVLG EVYPERDEES
 51 GAEQCEQDCR YRGEAVSDGF LSSLFGREIS SYTKEFLLDV QSRVNFTYRT
101 RFVPIARAPD GPSPLSLNLL VRTNPISTIE DYIANPDCFN TDIGWGCMIR
151 TGQSLLGNAL QILHLGRDFR VNGNESLERE SKFVNWFNDT PEAPFSLHNF
201 VSAGTELSDK RPGEWFGPAA TARSIQSLIY GFPECGIDDC IVSVSSGDIY
251 ENEVEKVFAE NPNSRILFLL GVKLGINAVN ESYRESICGI LSSTQSVGIA
301 GGRPSSSLYF FGYQGNEFLH FDPHIPQPAV EDSFVESCHT SKFGKLQLSE
351 MDPSMLIGIL IKGEKDWQQW KLEVAESAII NVLAKRMDDF DVSCSMDDVE
401 VSSNSMKKDA SNNENLGVLE GDYVDIGAIF PHTTNTEDVD EYDCFQDIHC
451 KKQKIVVMGN THTVNANLTD YEVEGVLVEK ETVGIHSPID EKC
```

b

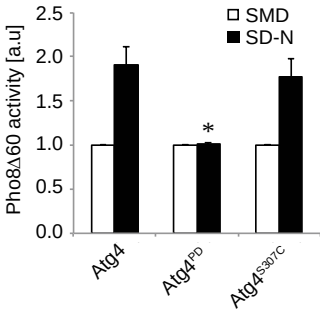

Supplementary Figure 1. Atg4 and amino acid sequence. (a) Atg4 contains 7 potential Atg1 phosphorylation sites. *Saccharomyces cerevisiae* Atg4 amino acid sequence. The potential phospho-acceptor serines in the Atg1 potential phosphorylation sites are in blue, S307 is in green and the residues that are putatively part of the catalytic site are in red. (b) The *atg4*Δ (SAY130) strain carrying a plasmid expressing Atg4, Atg4^{PD} or Atg4^{S307C} was grown in SMD or nitrogen starved (SD-N) for 3 h before measuring Pho8Δ60 activity in cell lysates. Pho8Δ60 activity was expressed in and a.u. stands for arbitrary units and relative to the control SMD conditions. Error bars represent the SD of 5 independent experiments. The symbol * indicates statistical significance ($p<0.001$) with the cells carrying Atg4 and was calculated with the paired two-tailed Student's t-test.

a

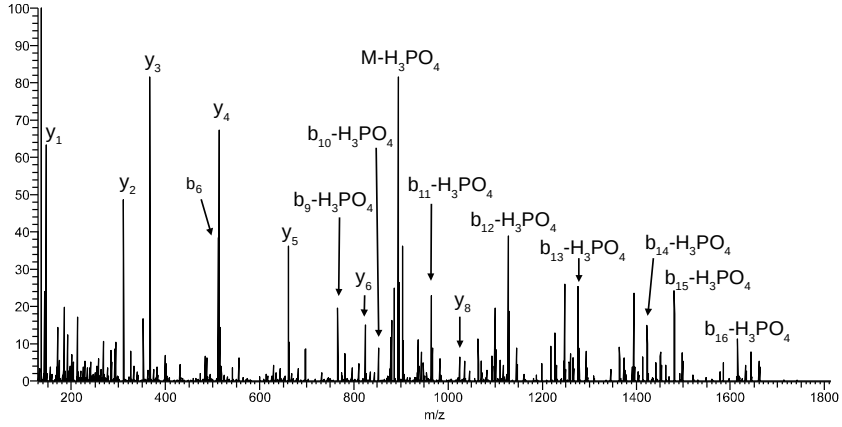

b

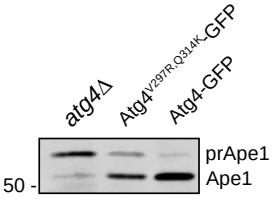

Supplementary Figure 2. Atg4 phosphorylation analysis *in vivo*. (a) $Atg4^{V297R,Q314KGFP}$ was purified and processed for protein mass spectrometry as described in Methods. Extracted ion chromatogram of the phosphorylated GIAGGRPSSSLYFFGYK peptide is presented. Proposed structures of the fragment ions are indicated with numbered letter. The detailed data are in Supplementary Table 2. (b) Normal progression of autophagy in cells overexpressing $Atg4^{V297R,Q314K}$ -GFP was assessed by monitoring maturation of precursor Ape1 (prApe1) into Ape1 by western blot. The *atg4*Δ strain transformed with an empty verctor (pRS416, *atg4*Δ), pTEFATG4-GFP(416) or pTEFAtg4V297R,Q314K-GFP(416), was grown to an exponential phase before precipitating proteins with trichloroacetic acid and separate them by SDS-PAGE. Western blot membranes were probed with anti-Ape1 antibodies.

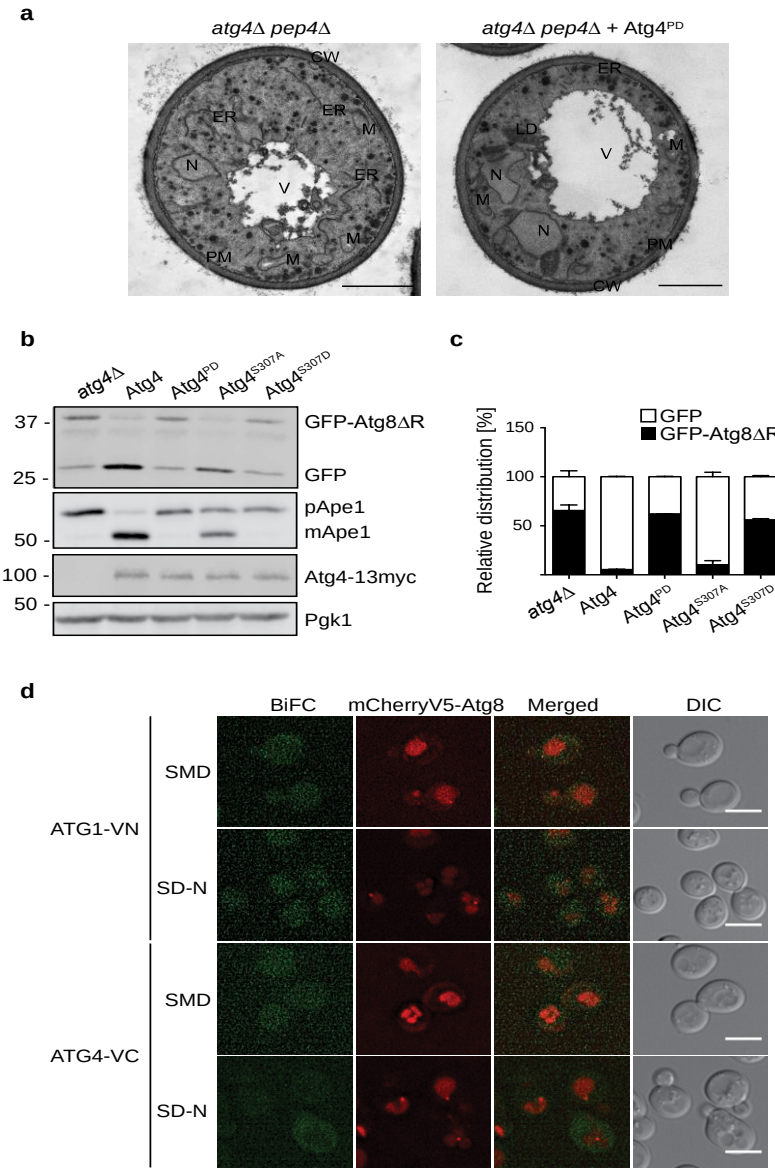

Supplementary Figure 3. Control experiments for electron microscopy, GFP-Atg8ΔR distribution analyses and BiFC assay. (a) The *atg4*Δ *pep4*Δ strain transformed with an empty plasmid (JSY163) or expressing Atg4^{PD}-GFP (SAY145) was processed for electron microscopy as in Fig. 1d. CW, cell wall; ER, endoplasmic reticulum; LD, Lipid droplet; M, mitochondrion; N, nucleus; PM, plasma membrane; V, vacuole. Scale bar, 1 µm. (b) TCA precipitated proteins from the cells analyzed in Fig. 2b were examined by western blot. (c) Quantification of the amounts of GFP-Atg8ΔR and GFP in the western blot shown in (b). Error bars

represent the SD of 3 independent experiments. (d) Control experiments for the BiFC assay. WT cells expressing endogenous Atg1-VN (JSY181) or Atg4-VC (JSY184) and carrying the pCumCherryV5ATG8(416) plasmid were processed as in Fig. 4a. DIC, differential interference contrast. Scale bar, 5 µm.

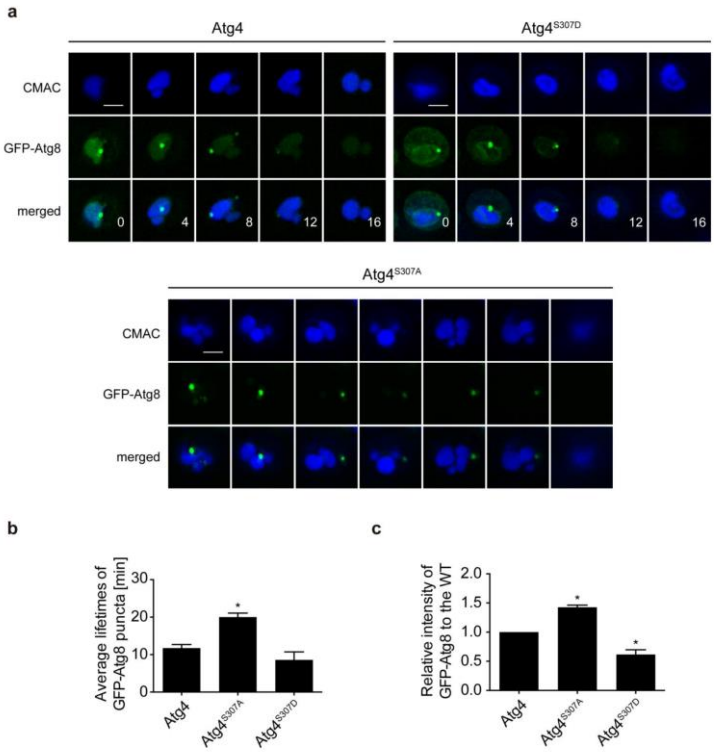

Supplementary Figure 4. Time-lapse imaging of GFP-Atg8ΔR-positive autophagosomes in presence of Atg4, Atg4^{S307D} and Atg4^{S307A}. (a) Cells expressing GFP-Atg8ΔR and Atg4 (RGS306), Atg4^{S307D} (RSY298) or Atg4^{S307A} (RGS297) were grown in YPD medium at 30˚C to a logarithmic phase before being after nitrogen starved in SD-N medium for 30 min. Cells were also incubated with the CMAC dye to label the vacuole, 10 min before being analysed by live-cell imaging as described in Methods with picture collected every 30 s. A representative event for each strain is shown in Supplementary Movies 1, 2 and 3. The single focal plane frames from these videos collected at the intervals of 4 min, are shown in the panel. Scale bar: 2 µm. (b) Quantification of GFP-Atg8ΔR-positive puncta lifetimes imaged in (a). Autophagosome formation time was define and measured from the appearance until disappearance of GFP-Atg8ΔR punctum over-time. Error bars indicate the SD of three independent experiments and in each experiment, 25 cells where the PAS was monitored continuously in the same confocal planes were

analyzed. Significant differences ($p<0.01$) between the various Atg4 mutants and the WT are indicated with the symbol *. (c) Fluorescence intensity quantification of GFP-Atg8ΔR punctate structures in the strains examined in (a). The average intensity of cells expressing WT Atg4 was set to 1 as relative reference. Error bars indicate the SD of three independent experiments. Significant differences ($p<0.01$) between the various Atg4 mutants and the WT are indicated with the symbol * and were calculated with the paired two-tailed Student's t-test.

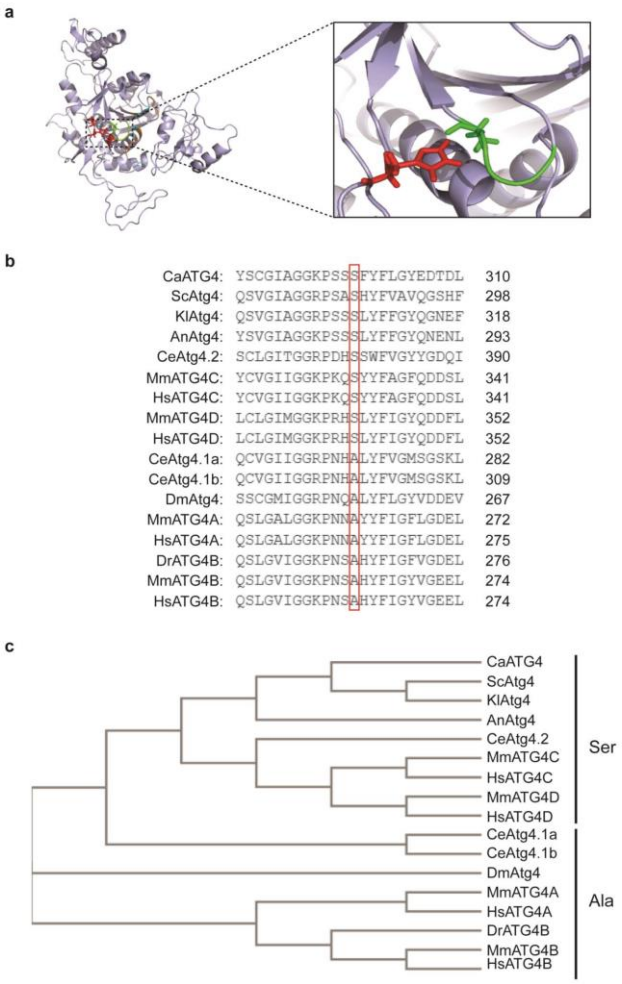

Supplementary Figure 5. Predicted three-dimensional model of yeast Atg4 structure and conservation of S307 among eukaryotes. (a) Three-dimensional model predicting yeast Atg4 structure generated from the crystal structure of human ATG4B using the software at http://robetta.bakerlab.org/ (left) and an enlargement of the inset highlighting the region around S307 (right). The putative catalytic site (C147, D322 and H324) of Atg4 is highlighted in red. The putative

regulatory loop is colored in green and conserved residues forming part of the predicted Atg8 interaction region are in light blue and orange. (b) Alignment of multiple amino acid sequences of Atg4 from different species was performed using the Clustal Omega software (http://www.ebi.ac.uk/Tools/msa/clustalo/). The residues in the equivalent position to the S307 of yeast Atg4 are highlighted by a red square. UniprotKB accession numbers are: *C. albicans* Atg4 (Q59UG3), *A. nidulans* Atg4 (Q5B7L0), *S. cerevisiae* Atg4 (P53867), *K. lactis* Atg4 (Q6CQ60), *C. elegans* Atg4.1a (Q9N30), *C. elegans* Atg4.1b (K8ESC5), C. elegans Atg4.2 (Q9U1N6), *D. melanogaster* Atg4 (M9PBM3), D. rerio Atg4B (Q6DG88), *M. musculus* ATG4A (Q8C9S8), *M. musculus* ATG4B (Q8BGE6), *M. musculus* ATG4C (Q811C2), *M. musculus* ATG4D (Q8BGV9), *H. sapiens* ATG4A (Q8WYN0), *H. sapiens* ATG4B (Q9Y4P1), *H. sapiens* ATG4C (Q96DT6) and *H. sapiens* ATG4D (Q86TL0). (c) Cladogram showing the phylogenetic relation among the Atg4 proteins from different eukaryotes obtained using the Clustal Omega software (http://www.ebi.ac.uk/Tools/msa/clustalo/). On the right of the figure it is indicated which Atg4 homologues have a serine (Ser) or an alanine (Ala) residue in the equivalent position to the S307 of yeast Atg4.

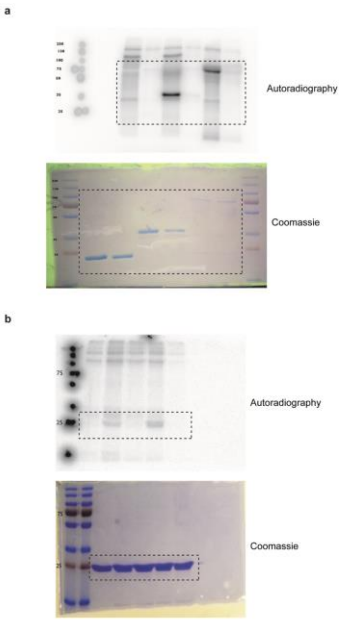

Supplementary Figure 6. Original material. (a) Autoradiography and scan used to generate Figure 1a. (b) Autoradiography and scan used to generate Figure 1c.

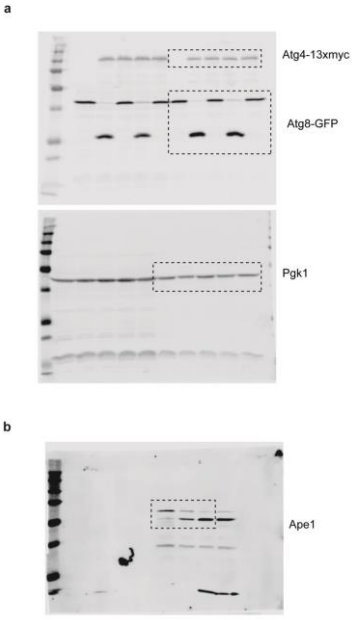

Supplementary Figure 7. Original material. (a) Scans of the western blots used to generate Figure 2a. (b) Scan of the western blots used to generate Supplementary Figure 2b.

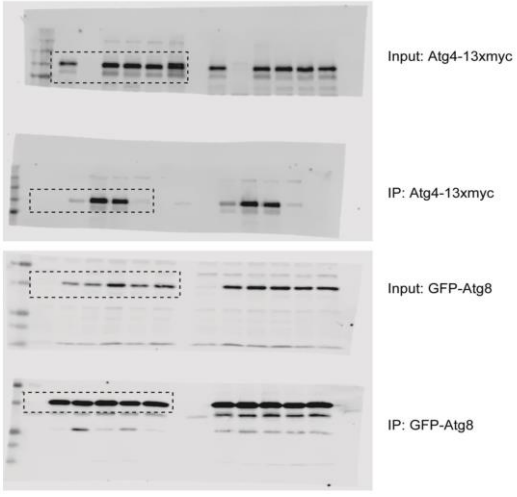

Supplementary Figure 8. Original material. Scans of the western blots used to generate Figure 3b.

Supplementary Table 1. Yeast strains used in this work

Name	Genotype	Origin
JSY151	SEY6210 *atg4Δ*::*TRP1 CUP1pr-GFP-ATG8ΔR*::*LEU2*	This study
JSY163	SEY6210 *atg4Δ*::*TRP1 pep4Δ*::*LEU2 pRS*::*URA3*	This study
JSY164	SEY6210 *atg4Δ*::*TRP1 pep4Δ*::*LEU2 ATG4^{S307A}-GFP*::*URA3*	This study
JSY165	SEY6210 *atg4Δ*::*TRP1 pep4Δ*::*LEU2 ATG4^{S307D}-GFP*::*URA3*	This study
JSY181	SEY6210 *ATG1-VN*::*HIS3*	This study
JSY184	SEY6210 *ATG4-VC*::*TRP1*	This study
JSY185	SEY6210 *ATG1-VN*::*HIS3 ATG4-VC*::*TRP1*	This study
JSY190	SEY6210 *atg2Δ*::*hphNTI ATG1-VN*::*HIS3 ATG4-VC*::*TRP1*	This study
JSY215	SEY6210 *atg2Δ*::*hphNTI atg13*::*LEU2 ATG1-VN*::*HIS3 ATG4-VC*::*TRP1*	This study
MNY006	SEY6210 *ATG4-GFP*::*TRP1*	This study
PJ69-4A	*MATα leu2-3,112 trp1-901 ura3-52 his3-200 gal4 gal80 LYS2*::*GAL1-HIS3 GAL2-ADE2 met2*::*GAL7-lacZ*	[35]
RGS297	SEY6210 *atg4Δ*::*TRP1 CUP1pr-GFP-ATG8ΔR*::*LEU2 pATG4^{S307A}*::*URA3*	This study
RGS298	SEY6210 *atg4Δ*::*TRP1 CUP1pr-GFP-ATG8ΔR*::*LEU2 pATG4^{S307D}*::*URA3*	This study
RGS306	SEY6210 *atg4Δ*::*TRP1 CUP1pr-GFP-ATG8ΔR*::*LEU2 pATG4*::*URA3*	This study
SAY084	SEY6210 *atg4Δ*::*TRP1*	This study
SAY114	SEY6210 *atg4Δ*::*TRP1 CUP1-ATG8-GFP*::*HIS3*	This study
SAY130	YTS159 *atg4Δ*::*HIS5 S.p*	This study
SAY144	SEY6210 *atg4Δ*::*TRP1 pep4Δ*::*LEU2 ATG4-GFP*::*URA3*	This study
SAY145	SEY6210 *atg4Δ*::*TRP1 pep4Δ*::*LEU2 ATG4^{PD}-GFP*::*URA3*	This study
SEY6210	*MATα ura3-52 leu2-3,112 his3-Δ200 trp1-Δ901 lys2-801 suc2- Δmel GAL*	[43]
YTS159	*MATα his3Δ1 leu2Δ0 lys2Δ0 ura3Δ0 pho13Δ*::*KAN pho8*::*PHO8Δ60*	[44]

Supplementary Table 2. Fragments of the phosphopeptide containing S307

Ion	Theoretical mass	Charge	Fragment	Error (ppm)	Observed mass	Intensity
y1	147,1128	1	y.K.	1,1	147,112965	29455,555
b2	171,1128	1	.GI.a	1,1	171,112991	6784,47
y2	310,1761	1	g.YK.	0,4	310,176245	22795,92
y3	367,1976	1	f.GYK.	0,4	367,19776	38706,972
b6	512,294	1	.GIAGGR.p	1,3	512,294621	18049,535
y4	514,266	1	f.FGYK.	1,2	514,266646	31481,249
y5	661,3344	1	y.FFGYK.	1,1	661,335124	16951,494
b9 -H3PO4	765,4002	1	.GIAGGRPSS.s [1xPhospho]	0,8	765,400814	9385,1363
y6	824,3978	1	l.YFFGYK.	-3,5	824,394839	7189,8417
b10 -H3PO4	852,4322	1	.GIAGGRPSSS.l [1xPhospho]	2,8	852,434598	4239,2025
a11 -H3PO4	937,5214	1	.GIAGGRPSSSL.y [1xPhospho]	5	937,526105	5226,2504
b11 -H3PO4	965,5163	1	.GIAGGRPSSSL.y [1xPhospho]	1,8	965,518006	10765,566
y8	1024,5138	1	s.SLYFFGYK.	1,4	1024,515319	3141,1023
b11	1063,4932	1	.GIAGGRPSSSL.y [1xPhospho]	1,2	1063,494449	5405,7069
y9 -H2O	1093,5353	1	s.SSLYFFGYK.	1,9	1093,537427	3142,459
a12 -H3PO4	1100,5847	1	.GIAGGRPSSSLY.f [1xPhospho]	0,4	1100,58518	9392,8115
b12 -H3PO4	1128,5796	1	.GIAGGRPSSSLY.f [1xPhospho]	1	1128,580742	18525,648
b12	1226,5565	1	.GIAGGRPSSSLY.f [1xPhospho]	0,9	1226,557631	6077,6881
a13 -H3PO4	1247,6531	1	.GIAGGRPSSSLYF.f [1xPhospho]	0,7	1247,654062	12089,635
b13 -H3PO4	1275,648	1	.GIAGGRPSSSLYF.f [1xPhospho]	0,9	1275,649207	12113,115
b13	1373,6249	1	.GIAGGRPSSSLYF.f [1xPhospho]	2,5	1373,6284	2952,5813
a14 -H3PO4	1394,7215	1	.GIAGGRPSSSLYFF.g [1xPhospho]	1	1394,722916	11252,16
b14 -H3PO4	1422,7165	1	.GIAGGRPSSSLYFF.g [1xPhospho]	1,6	1422,718782	7187,6221
a15 -H3PO4	1451,743	1	.GIAGGRPSSSLYFFG.y [1xPhospho]	-0,4	1451,742493	3650,5025
b15 -H3PO4	1479,7379	1	.GIAGGRPSSSLYFFG.y [1xPhospho]	1,2	1479,739648	11264,852
b15	1577,7148	1	.GIAGGRPSSSLYFFG.y [1xPhospho]	2,3	1577,718519	1173,9552
a16 -H3PO4	1614,8063	1	.GIAGGRPSSSLYFFGY.k [1xPhospho]	0,9	1614,807866	5342,8832
b16 -H3PO4	1642,8013	1	.GIAGGRPSSSLYFFGY.k [1xPhospho]	0,4	1642,801956	3685,3678